REAL-TIME RESOLUTION OF CONFLICTING OBJECTIVES IN BUILDING ENERGY MANAGEMENT: AN UTOPIA-TRACKING APPROACH*

Victor M. Zavala
Mathematics and Computer Science Division
Argonne National Laboratory, Argonne, IL

ABSTRACT

We present an *utopia-tracking* multiobjective optimization strategy to resolve conflicting objectives in real-time energy management. Conflicts arise frequently from the need to balance economic and noneconomic metrics such as energy demand and occupant comfort. We demonstrate that the proposed approach leads to better performance compared with the traditional weighting approach. In particular, we demonstrate that improper adjustment of weights can lead to large excursions in performance. The proposed approach automatically locates the optimal weights and does not require the computation of the Pareto front, making it ideal for real-time implementation.

INTRODUCTION

Optimization-based energy management is becoming commonplace (Zavala et al. 2010; Kolokotsa et al. 2009; K. Marik and Vass 2011; Ward et al. 2008; Henze, Felsmann, and Knabe 2004; Oldewurtel et al. 2010; Mahdavi 2001; Huang and Lam 1997). These systems use a building model coupled to an optimization engine to compute optimal operating conditions that minimize/maximize a given performance objective as internal and external building conditions change in time. A problem faced by these systems is that they need to balance economic metrics with metrics that do not have a direct translation to economic value, such as occupant thermal comfort and health (e.g., air quality). Other metrics typical in control systems include robustness (e.g., constraint violation) and equipment wearing (e.g., actuators).

Thermal comfort is typically controlled by forcing the control system to track temperature and relative humidity set-points as tightly as possible. Computationally, this is achieved by tuning the relative weights of the comfort and energy objectives in the optimization formulation. We claim that this approach can seriously impact performance when the Pareto front is steep (improving one objective strongly affects the other). In addition, the weights strongly depend on the building conditions. Consequently, fixing weights throughout daily, weekly, and seasonal cycles can lead to large excursions in performance. Another issue is that existing approaches determine optimal weights by constructing the Pareto front and then selecting an appropriate set of weights from it. Such

approach can be computationally prohibitive, particularly in real-time decision-making.

We present a utopia-tracking strategy to handle the limitations of weighting-based multiobjective optimization. The approach automatically determines the point along the Pareto front of minimum distance to to the so-called utopia point. The utopia point is, as the name suggests, an *ideal* point given by the intersection of the objective values obtained when each objective is minimized independently without taking into account the rest of the conflicting objectives. The proposed approach requires only the coordinates of the utopia point to determine the weights corresponding to the minimum distance solution along the Pareto front to the utopia point. Since the approach does not require the construction of the Pareto front, it is suitable for real-time implementation. In a numerical study, we demonstrate that the proposed strategy can optimally resolve conflicts between energy demand and comfort and can handle steep Pareto fronts efficiently.

MULTIOBJECTIVE OPTIMIZATION

Consider the multiobjective optimization problem:

$$\min_x \; [\Phi_1(x,\omega), \Phi_2(x\omega,), ..., \Phi_M(x,\omega)] \qquad (1a)$$

$$\text{s.t.} \; g(x,\omega) \leq 0. \qquad (1b)$$

Here, the objectives or cost functions are given by $\Phi_i : \mathbb{R}^{n_x \times n_\omega} \to \mathbb{R}$, $i \in \mathcal{M} := \{1, ..., M\}$ where $x \in \mathcal{R}^{n_x}$ are the system variables (i.e., states and degrees of freedom) and $\omega \in \mathcal{R}^{n_\omega}$ is the problem data (i.e., weather and costs). The constraints are given by the function vector $g : \mathbb{R}^{n_x \times n_\omega} \to \mathbb{R}^m$. We define the cost vector as

$$\Phi(\cdot,\cdot)^T := [\Phi_1(\cdot,\cdot), \Phi_2(\cdot,\cdot), ..., \Phi_M(\cdot,\cdot)]^T. \qquad (2)$$

When the cost functions are conflicting, one cannot be minimized without increasing the other. This situation gives rise to the concept of a *Pareto solution*. A feasible point x_p for the multiobjective problem (1) is said to be Pareto optimal if and only if no other feasible point x exists such that $\Phi_i(x) \leq \Phi_i(x_p), \forall i \in \mathcal{M}$ and $\Phi_i(x) < \Phi_i(x_p)$ for at least one index $i \in \mathcal{M}$. The family of Pareto solutions forms the so-called Pareto front, which represents a limiting curve of performance in the cost space. In other words, no feasible point can lie below the Pareto front.

A traditional approach to resolve conflicting objectives is to construct the Pareto front and then choosing a suit-

able point along it (Kerrigan et al. 2000). The Pareto front is typically constructed by following an ε-constraint approach. In the case of two objectives, a domain for the first objective is assumed $[\Phi_1^L \Phi_1^U]$ and discretized by using $j = 1, .., T$ points denoted by Φ_1^j. In order to determine the corresponding coordinates of the Pareto front for the second objective, Φ_2^j, the following optimization problem is solved:

$$\min_x \quad \Phi_2(x, \omega) \tag{3a}$$

$$\text{s.t. } g(x, \omega) \leq 0 \tag{3b}$$

$$\Phi_2(x, \omega) \geq \Phi_1^j, \tag{3c}$$

for $j = 1, .., T$. Since the objectives are conflicting, Φ_1^j acts as a blocking constraint, and (Φ_1^j, Φ_2^j) is a Pareto point. An equivalent approach that works well when objectives are well-scaled is to select a set of weights w^j by discretizing the domain $[0, 1]$ in $j = 1, .., T$ points and solve the problem

$$\min_x \quad w^j \cdot \Phi_1(x, \omega) + (1 - w^j) \cdot \Phi_2(x, \omega) \tag{4a}$$

$$\text{s.t. } g(x, \omega) \leq 0. \tag{4b}$$

The resulting solution $\Phi_1(x, \omega), \Phi_2(x, \omega)$ is a Pareto solution.

We highlight that the shape of the Pareto front and its dependency on the data ω are entirely problem-dependent. This is one of the main reasons why the decision-maker is typically interested in constructing it. Once the Pareto front is constructed, the decision-maker or *expert* selects a point along the Pareto front by selecting a weight w^j. Many criteria are typically used to select such a point. Intuitively, the expert would like to select the weight that is the closest to the *limiting* performance of the system. This point is given by the *utopia point*. The utopia is a point given by the solution (x_i^L) with coordinates $\Phi_i^L = \Phi_i(x_i^L)$ in the cost space. The coordinates are given by the solution of the problems

$$\min_x \Phi_i(x) \text{ s.t. } g(x, \omega) \leq 0, \tag{5}$$

for $i \in \mathcal{M}$. We see that the utopia point is *unattainable* because it is not possible to minimize one objective without increasing the others. Consequently, this point lies below the Pareto front. To get close to the limiting performance, the expert can choose the weight corresponding to the point along the Pareto front that is closest to the utopia point. Such a point is known as the *compromise solution*. We denote this solution as x^c with cost coordinates $\Phi_i(x^c)$, $i \in \mathcal{M}$. The location of the utopia and compromise points is illustrated in Figure 1. The choice of the compromise solution as the point of choice is not strictly necessary. Other possibilities include the Kalai-Smorodinsky
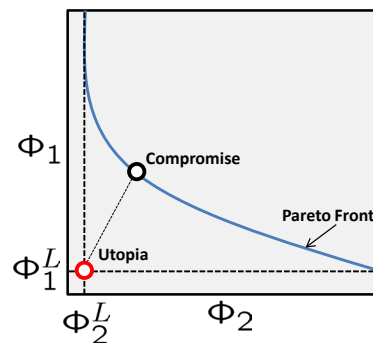

Figure 1: Schematic representation of Pareto front, compromise solution, and utopia point.

solution, the egalitarian solution, and the Nash solution (Gambier 2008).

Unfortunately, selecting weights by constructing the Pareto front can become extremely computationally expensive because they require the solution of many optimization problems. This is specially true if the Pareto front is *steep*. Steep profiles arise when one objective strongly increases as another one decreases. This is illustrated in Figure 2. When a steep profile is encountered, a large number of discretized points are needed to capture the shape of the front. As expected, a coarse discretization can lead to suboptimal performance because the weight selected by the expert can be misplaced. Note also that as the Pareto front becomes steeper, the penalty paid by moving away from the compromise solution increases. Consequently, misplacement of weights due to discretization errors can significantly increase performance.

In the presence of more than two objectives, the complexity of constructing the Pareto front increases exponentially because discretizing the domain requires an exponentially increasing number of points. Consequently, constructing the Pareto front is not appropriate for time-critical environments such as energy management.
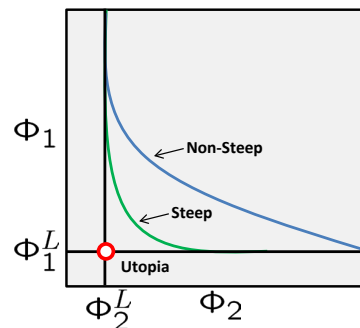

Figure 2: Steep and nonsteep Pareto fronts.

UTOPIA-TRACKING APPROACH

Assume that the utopia cost coordinate vector is given by $\Phi^L = [\Phi_1(x_1^L),...,\Phi_M(x_M^L)]$. A key observation is that it is possible to compute the cost coordinates of the compromise solution directly by solving the problem

$$\min_x \|\Phi(x,\omega) - \Phi^L\|_p \text{ s.t. } g(x,\omega) \leq 0. \quad (6)$$

Here, $\|\cdot\|_p$ is the p-norm. The coordinates of the compromise solution are given by $\Phi_i(x^c)$, $i \in \mathcal{M}$. We will denote the above problem as the *utopia-tracking problem*. A schematic representation of the utopia-tracking approach is presented in Figure 1. Note that, for the single-objective case, the compromise solution and the utopia point coincide so that $\Phi_1(x) = \Phi_1^L$.

The p-norm $\|\cdot\|_p$ with $p \geq 1$ has the general form

$$\|s\|_p = \left(\sum_{i=1}^{n_s} |s_i|^p\right)^{\frac{1}{p}}, \quad (7)$$

for vector $s \in \mathbb{R}^{n_s}$ with elements s_i, $i = 1,...,n_s$. We have that with $\|s\|_p = 0$ if $s = 0$ and $\|s\|_p > 0$ otherwise for all $p \geq 1$. Well-known norms are the $\mathcal{L}_1, \mathcal{L}_2$ and the $\mathcal{L}_\infty$ norms:

$$\|s\|_1 = \sum_{i=1}^{n_s} |s_i| \quad (8a)$$

$$\|s\|_2 = \sqrt{\sum_{i=1}^{n_s} (s_i)^2} \quad (8b)$$

$$\|s\|_\infty = \max\{|s_1|,...,|s_{n_s}|\}. \quad (8c)$$

The choice of norm defines the location of the compromise solution. The difference in position is exacerbated by the difference in magnitude (scaling) of each of the objectives. Also, the choice of the norm has important implications on computational performance. For instance, the $\mathcal{L}_2$ norm is smooth (differentiable), whereas $\mathcal{L}_1$ and $\mathcal{L}_\infty$ are not.

To ameliorate the scaling issue, we note that the solution of the individual problems (5) also yields upper bounds Φ_i^U, $i \in \mathcal{M}$, given by the costs not minimized. Consequently, we can use these to scale the cost distances without affecting its properties. The scaled $\mathcal{L}_2$ problem has the form

$$\min_x \left\|\frac{\Phi(x,\omega) - \Phi^L}{\Phi^U - \Phi^L}\right\|_2 \quad (9a)$$

$$\text{s.t. } g(x,\omega) \leq 0. \quad (9b)$$

The square root in the objective function can introduce numerical ill-conditioning because the first derivative diverges as the argument approaches zero. To deal with this problem, we can use the formulation

$$\min_{x,z} \quad z \quad (10a)$$

$$\text{s.t. } g(x,\omega) \leq 0 \quad (10b)$$

$$z^2 = \sum_{i \in \mathcal{M}} \left(\frac{\Phi_i(x,\omega) - \Phi_i^L}{\Phi_i^U - \Phi_i^L}\right)^2 \quad (10c)$$

$$z \geq 0, \quad (10d)$$

which is better-conditioned. Another popular approach is to minimize the squared form of the norm.

To reformulate the $\mathcal{L}_1$ variant, we note that $\Phi_i(x^c,\omega) \geq \Phi_i^L$, $i \in \mathcal{M}$ and for all (x,ω). Consequently, we can eliminate the absolute value to obtain,

$$\min_x \quad \sum_{i \in \mathcal{M}} \frac{\Phi_i(x,\omega) - \Phi_i^L}{\Phi_i^U - \Phi_i^L} \quad (11a)$$

$$\text{s.t. } g(x,\omega) \leq 0. \quad (11b)$$

We can reformulate the $\mathcal{L}_\infty$ variant as follows. We first note that any problem of the form $\min_z \|z\|_\infty$ with variable vector $z = [z_1,...,z_M]$ can be reformulated as $\min_{z,\eta} \quad \eta \quad \text{s.t.} \quad |z_i| \leq \eta, \quad i \in \mathcal{M}$. If $z_i = \Phi_i(x,\omega) - \Phi_i^L$, we can see that $z_i \geq 0$ because $\Phi_i(x,\omega) \geq \Phi_i^L$. Consequently, as before, the absolute value is not needed. We thus have

$$\min_{x,\eta} \quad \eta \quad (12a)$$

$$\text{s.t. } g(x,\omega) \leq 0 \quad (12b)$$

$$\frac{\Phi_i(x,\omega) - \Phi_i^L}{\Phi_i^U - \Phi_i^L} \leq \eta, \quad i \in \mathcal{M}. \quad (12c)$$

NUMERICAL STUDY

We present a numerical study to illustrate the concepts. We construct a multiobjective optimal control problem using an aggregated first-principles model of a building to demonstrate that the energy demand-comfort Pareto front can be highly steep, and we determine the location of the utopia and compromise points. All the codes used for the calculations can be accessed at `http://www.mcs.anl.gov/~vzavala/publications.html`.

SYSTEM MODEL

For our optimization studies, we consider a model describing the dynamics of a building space conditioned by an air-handling unit (AHU) system. The system is sketched in Figure 3. We capture the building conditions in terms of CO_2 concentration, humidity, pressure, and temperature. The model nomenclature is provided in the appendix.
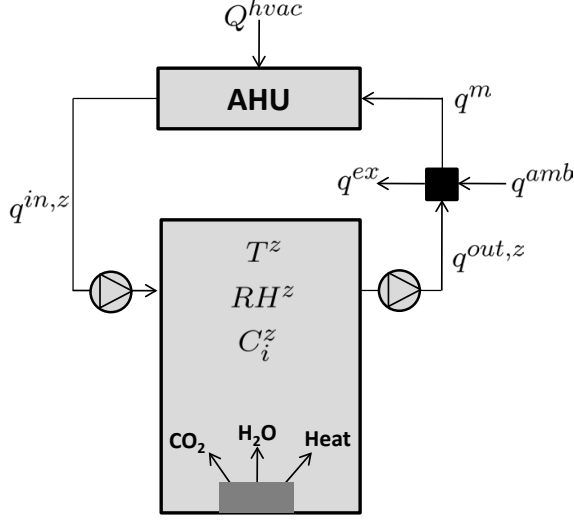
Figure 3: Schematic representation of building system.

Material Balances

In the building envelope we have the total mass balance,

$$\frac{dm^z(\tau)}{d\tau} = \rho \cdot \left(q^{in,z}(\tau) - q^{out,z}(\tau) \right), \quad (13)$$

where τ is time. We also have the component balances,

$$V^z \cdot \frac{dC_i^z(\tau)}{d\tau} = q^{in,z}(\tau) \cdot C_i^{in,z}(\tau) - q^{out,z}(\tau) \cdot C_i^z(\tau)$$
$$+ n(\tau) \cdot n_{tot} \cdot G_i^z, \; i \in \{CO_2, H_2O\}. \quad (14)$$

Here, $n(\tau)$ is the occupancy signal of the space (value of one if the space is occupied and zero if it is unoccupied). The total number of occupants under occupied mode is given by n_{tot}. Assuming constant density and heat capacity in the mixer, we have

$$q^{out,z}(\tau) + q^{amb}(\tau) = q^{ex}(\tau) + q^m(\tau) \quad (15a)$$
$$C_i^z(\tau) \cdot q^{out,z}(\tau) + C_i^{amb}(\tau) \cdot q^{amb}(\tau) =$$
$$C_i^z(\tau) \cdot q^{ex}(\tau) + C_i^m \cdot q^m(\tau), \; i \in \{CO_2, H_2O\}. \quad (15b)$$

In the AHU, we have the following balances:

$$q^{z,in}(\tau) = q^m(\tau) \quad (16a)$$
$$m_i^{rm}(\tau) = q^{in,z}(\tau) \cdot C_i^{in,z}(\tau) - q^m(\tau) \cdot C_i^m(\tau), \quad (16b)$$

$i \in \{CO_2, H_2O\}$. Here, $m_i^{rm}(\cdot)$ are the mass removal rates with $m_{CO_2}^{rm}(\cdot) = 0$ since this component is not removed in the AHU. The relationship between the total building pressure, mass, and temperature can be estimated from the ideal gas law:

$$P^z(\tau) = \frac{m^z(\tau) \cdot R \cdot T^z(\tau)}{M \cdot V^z}. \quad (17)$$

We convert the relative humidity of the air at the building temperature $T^z(\tau)$ to volumetric concentration $C_{H_2O}^z(\tau)$ using the following relationship

$$RH^z(\tau) = 100 \cdot \frac{C_{H_2O}^z(\tau)}{C_{H_2O}^{sat}(\tau)}, \quad (18)$$

where the saturation concentration is given by Antoine's equation (Reid, Prausnitz, and Poling 1987)

$$\log_{10}(C_{H_2O}^{sat}(\tau)) = 8.07131 - \frac{1730.63}{T^z(\tau) - 39.73}. \quad (19)$$

We can convert the volumetric concentration of CO_2 to ppmV (typical metric for air quality) using the relationship (epappmv 2011),

$$ppmV_{CO_2}^z(\tau) = 1000 \cdot \frac{C_{CO_2}^z(\tau) \cdot R \cdot T^z(\tau)}{M_{CO_2} \cdot P^z(\tau)}. \quad (20)$$

Energy Balances

We consider the following energy balance for the building envelope (Tashtoush, Molhim, and Al-Rousan 2005):

$$m^z(\tau) \cdot c_p \cdot \frac{dT^z(\tau)}{dt} =$$
$$q^{in,z}(\tau) \cdot \rho \cdot c_p \cdot T^{in,z}(\tau) - q^{out,z}(\tau) \cdot \rho \cdot c_p \cdot T^z(\tau)$$
$$- U^w \cdot A^w \cdot (T^z(\tau) - T^{amb}(\tau)) + n(\tau) \cdot n_{tot} \cdot Q^z. \quad (21)$$

In the mixer we have

$$q^{out,z}(\tau) \cdot T^z(\tau) + q^{amb}(\tau) \cdot T^{amb}(\tau) =$$
$$q^{ex}(\tau) \cdot T^z(\tau) + q^m(\tau) \cdot T^m(\tau). \quad (22)$$

The amount of condensate in the AHU is proportional to the latent energy removed/added:

$$Q^{lat}(\tau) = h^{lat} \cdot m_{H_2O}^{rm}(\tau). \quad (23)$$

The amount of sensible energy removed/added in the AHU is given by

$$Q^{sens}(\tau) = q^{in,z}(\tau) \cdot \rho \cdot c_p \cdot (T^{in,z}(\tau) - T^m(\tau)). \quad (24)$$

The total energy consumed by the HVAC system is given by

$$Q^{hvac}(\tau) = |Q^{lat}(\tau)| + |Q^{sens}(\tau)|. \quad (25)$$

For computational efficiency, we replace the non-differentiable absolute value operator $|\cdot|$ using dummy variables as

$$Q^{hvac}(\tau) = Q_+^{lat}(\tau) + Q_-^{lat}(\tau) + Q_+^{sens}(\tau) + Q_-^{sens}(\tau) \quad (26a)$$

$$Q^{lat}(\tau) = Q_+^{lat}(\tau) - Q_-^{lat}(\tau) \quad (26b)$$
$$Q^{sens}(\tau) = Q_+^{sens}(\tau) - Q_-^{sens}(\tau), \quad (26c)$$

with $Q_+^{lat}(\tau), Q_-^{lat}(\tau), Q_+^{sens}(\tau), Q_-^{sens}(\tau) \geq 0$.

Degrees of Freedom and Constraints

If we assume a fixed pressure $P^z(\tau) = P^z$ we have that $q^{in,z}(\tau) = q^{out,z}(\tau)$, so that $m^z(\tau)$ is constant and $q^{amb}(\tau) = q^{ex}(\tau)$. In this case, the system has three operational degrees of freedom. The first degree of freedom can be either $q^{amb}(\tau)$ or $q^{ex}(\tau)$ but not both. The other two degrees of freedom can be the supply air temperature $T^{in,z}(\tau)$, or $Q^{sens}(\tau)$ and the supply air humidity, or $Q^{lat}(\tau)$. If we relax the constant pressure constraint through a *soft constraint* of the form

$$P_L \leq P(\tau) \leq P_U, \tag{27}$$

then the system has four degrees of freedom. Since this approach gives more flexibility for optimization, it is used here.

We impose temperature and humidity constraints of the form

$$T_L^z \leq T^z(\tau) \leq T_U^z \tag{28a}$$
$$RH_L^z \leq RH^z(\tau) \leq RH_U^z. \tag{28b}$$

Here, $T_L^z, RH_L^z, T_U^z, RH_U^z$ are nominal lower and upper bounds.

We consider constraints on air quality of the form

$$ppmV_{CO_2}^z(\tau) \leq ppmV_{CO_2,U}^z. \tag{29}$$

A lower bound is not necessary because this is given by the ambient concentration. Dampers represent an important dynamic constraint because of their slow dynamics. In other words, they cannot be moved freely because of physical limitations or equipment wearing. We model this limitations by using *ramp* constraints of the form,

$$\left| \frac{dq^{in,z}(\tau)}{d\tau} \right| \leq \Delta q_U^{in,z} \tag{30a}$$

$$\left| \frac{dq^{out,z}(\tau)}{d\tau} \right| \leq \Delta q_U^{out,z} \tag{30b}$$

$$\left| \frac{dq^m(\tau)}{d\tau} \right| \leq \Delta q_U^m \tag{30c}$$

$$\left| \frac{dq^{amb}(\tau)}{d\tau} \right| \leq \Delta q_U^{amb} \tag{30d}$$

$$\left| \frac{dq^{ex}(\tau)}{d\tau} \right| \leq \Delta q_U^{ex}. \tag{30e}$$

We impose operational bounds on the AHU delivery temperature and physical bounds on the flow rates:

$$T_L^{in,z} \leq T^{in,z}(\tau) \leq T_U^{in,z} \tag{31a}$$
$$q_L^{in,z} \leq q^{in,z}(\tau) \leq q_U^{in,z} \tag{31b}$$
$$q_L^{out,z} \leq q^{out,z}(\tau) \leq q_U^{out,z} \tag{31c}$$
$$q_L^{ex} \leq q^{ex}(\tau) \leq q_U^{ex} \tag{31d}$$
$$q_L^m \leq q^{amb}(\tau) \leq q_U^m. \tag{31e}$$

Moreover, we consider initial conditions for the dynamic states of the system:

$$m^z(t) = m_{init}^z \tag{32a}$$
$$T^z(t) = T_{init}^z \tag{32b}$$
$$C_i^z(t) = C_{i,init}^z, \ i \in \{CO_2, H_2O\}. \tag{32c}$$

Objectives

We consider a trade-off between energy demand and thermal comfort. The accumulated energy demand over a time horizon $\tau \in [t, t+T]$ is given by

$$\Phi_1 = \int_t^{t+T} Q^{hvac}(\tau) d\tau. \tag{33}$$

We consider a competing comfort objective of the form

$$\Phi_2 = \int_t^{t+T} \left(\|T^z(\tau) - T^{com}\|^2 + \|RH^z(\tau) - RH^{com}\|^2 \right) d\tau, \tag{34}$$

where T^{com} and RH^{com} define the desired comfort point for temperature and relative humidity, respectively. An alternative way of enforcing comfort is using the predicted mean vote (PMV) and predicted percentage dissatisfied (PPD) indexes (Olesen and Brager 2004). If a PPD metric is used to measure comfort, then PPD can be used directly as the competing objective $\Phi^2 = \int_t^{t+T} PPD \, d\tau$.

NUMERICAL RESULTS

To solve the resulting optimal control problems given by objectives (33)-(34) and constraints (13)-(32), we applied an implicit Euler discretization scheme to convert the problem into a nonlinear optimization problem. Time steps of one hour were used and we used IPOPT (Wächter and Biegler 2006) to solve the resulting problems and implemented the problems in the AMPL modeling language (Fourer, Gay, and Kernighan 1993). We used real ambient temperature and relative humidity data for three days in the month of March, 2006 in the Chicago area. The profiles are presented in Figure 4.

We constructed the Pareto front using an ε-constrained approach. In Figure 5, we present a Pareto front of energy demand against comfort error for an horizon of 3 days. Here, comfort is measured as the squared error from a desired reference point of 22^oC and 50% relative humidity as in equation (34). This corresponds to a PPD of 5.1%. We scaled the comfort error to stay within the range (0-10). As can be seen, the Pareto curve is highly steep at tight comfort conditions (e.g., a small change in comfort translates in large amounts of energy). One conclusion from the shape of the Pareto front is that enforcing comfort strictly (by adding large weights) is dangerous since it can lead to extremely high energy demand. In particular, from the graph we can see that a comfort error of around 0.2 (tight tracking of the $22^oC, 50\%$ point) gives
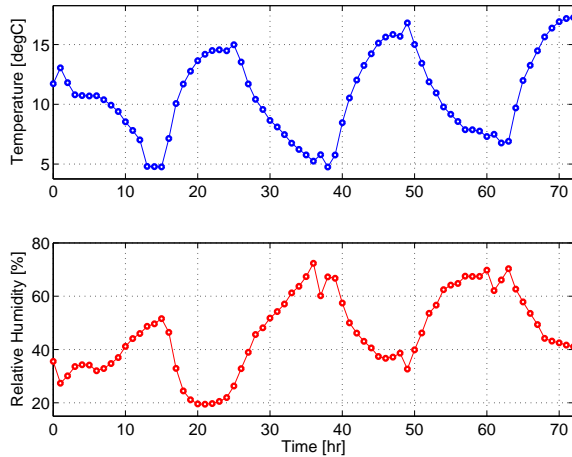
Figure 4: Ambient temperature and relative humidity profiles used in study.

Figure 5: Comfort-energy Pareto front, utopia point, and compromise solution.

an energy demand of nearly 5,000 kW, whereas allowing a small drift of the error (i.e., an average *dynamic* drift from 22^oC to 23^oC and humidity from 50%to 55%) can bring down the energy demand to levels of 2,500 kWh. This gives energy savings of 50%.

The impact of allowing temperature drifts from fixed comfort set-points on energy savings was also analyzed in (Zavala et al. 2011). The shape of the Pareto front presented here reinforces the observation that it is necessary to exploit the flexibility of the comfort zone in order to save energy. This also indicates that it is inefficient to tune control loops (PID loops) to track set-points with minimum error since, as demonstrated by the steepness of Pareto front, this can lead to large energy inefficiencies. This highlights the need for supervisory controllers (optimization-based energy management) capable of positioning thermostat and humidity set-points to optimally trade-off comfort and energy demands.

The proposed utopia-tracking strategy locates the utopia point and the compromise solution to compute the optimal trade-off point at the current real-time conditions. Note that the utopia energy demand (unattainable) is around 2,000 kWh, given by the limit in which comfort is fully relaxed. This also represents the absolute minimum energy demand needed to keep the building within the required bounds which are given by other operational priorities such as moisture control or prevention of equipment freezing. The energy demand of the compromise solution (optimal) is around 2,500 kWh. *This indicates that the cost of comfort is* 500 *kWh.*

We found that the $\mathcal{L}_\infty$ norm is numerically more robust and handles scaling issues efficiently. The construction of the Pareto front required a total of 100 optimization problems to define the steep section of the front. This required
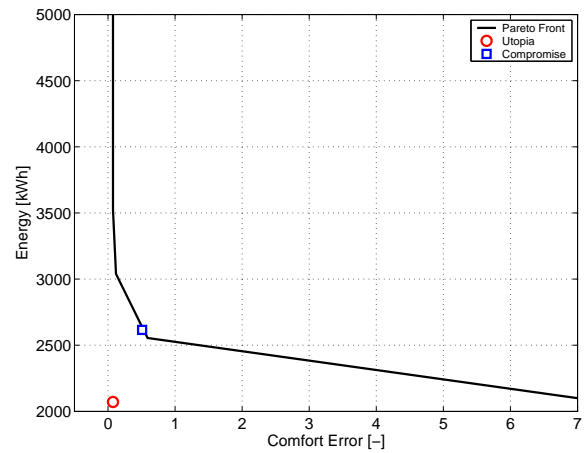
approximately one hour of computation in a standard personal computer. As can be seen from Figure 5, a hundred points do not provide sufficient resolution near the compromise point. We found that over 1,000 discretization points are needed to keep the resolution nearly constant. This would require ten hours of computation. The computation of the compromise point using the utopia-tracking approach required the solution of three optimization problems. Two problems were solved to identify the coordinates of the utopia point, and one was solved to locate the compromise solution. Less than two minutes were required for this computation. This indicates that the approach can be deployed in real-time strategies such as receding-horizon energy management and predictive control.

The proposed approach can be applied to any multi-objective problem arising in energy systems. Additional objectives include energy cost, which tends to shift demand to exploit price structures instead of minimizing energy demand. A problem arising in this setting is that energy demand can, in fact, increase, thus affecting indirect emissions. Another typical conflict is equipment wearing. Operators prefer to keep the system set-points fixed in order to minimize damper wearing and potential faults, but doing so increases energy demands and costs. The proposed framework can be used to resolve this conflict.

CONCLUSIONS AND FUTURE WORK

We present an utopia-tracking multiobjective optimization strategy to resolve conflicting objectives in real-time energy management. We demonstrate that the proposed approach leads to better performance compared with the traditional weighting approach. We also show that improper adjustment of weights can lead to large excursions

in performance. The proposed approach automatically locates the optimal weights and does not require the computation of the Pareto front, making it ideal for real-time implementation.

As part of future work, it would be interesting to perform more detailed numerical studies with changing weather and occupancy conditions during daily, weekly, and seasonal cycles.

ACKNOWLEDGMENTS

REFERENCES

Aglan, H. 2003. "Predictive model for CO_2 generation and decay in building envelopes." *Journal of Applied Physics* 93:1287–1290.

epappmv. 2011. "EPA On-line Tools for Site Assessment Calculation."

Fourer, R., D. Gay, and B. Kernighan. 1993. *AMPL*. South San Francisco: The Scientific Press.

Gambier, A. 2008. "MPC and PID Control Based on Multi-objective Optimization." *Proceedings of the American Control Conference*, pp. 4727–4732.

Henze, Gregor P., Clemens Felsmann, and Gottfried Knabe. 2004. "Evaluation of optimal control for active and passive building thermal storage." *International Journal of Thermal Sciences* 43 (2): 173 – 183.

Huang, W., and H.N. Lam. 1997. "Using genetic algorithms to optimize controller parameters for HVAC systems." *Energy and Buildings* 26 (3): 277 – 282.

Kerrigan, E., A. Bemporad, D. Mignone, M. Morari, and J. M. Maciejowski. 2000. "Multi-objective Prioritisation and Reconfiguration for the Control of Constrained Hybrid Systems." *Proceedings of the American Control Conference*, pp. 1694–1698.

K. Marik, J. Rojicek, P. Stluka, and J. Vass. 2011. "Advanced HVAC Control: Theory vs. Reality." *Proceedings of 18th IFAC World Congress*, pp. 3108–3113.

Kolokotsa, D., A. Pouliezos, G. Stavrakakis, and C. Lazos. 2009. "Predictive control techniques for energy and indoor environmental quality management in buildings." *Building and Environment* 44 (9): 1850 – 1863.

Mahdavi, Ardeshir. 2001. "Simulation-based control of building systems operation." *Building and Environment* 36 (6): 789 – 796.

Oldewurtel, F., A. Parisio, C.N. Jones, M. Morari, D. Gyalistras, M. Gwerder, V. Stauch, B. Lehmann, and K. Wirth. 2010, 30 2010-july 2. "Energy efficient building climate control using Stochastic Model Predictive Control and weather predictions." *American Control Conference (ACC), 2010*. 5100 – 5105.

Olesen, B. W., and G. S. Brager. 2004. "A Better Way to Predict Comfort: The New ASHRAE Standard 55-2004." *ASHRAE Journal*, pp. 20–26.

Reid, R. .C., J. M. Prausnitz, and B. E. Poling. 1987. *The properties of gases and liquids*. McGraw-Hill.

Tashtoush, Bourhan, M. Molhim, and M. Al-Rousan. 2005. "Dynamic model of an HVAC system for control analysis." *Energy* 30 (10): 1729 – 1745.

Wächter, A., and L. T. Biegler. 2006. "On the Implementation of a Primal-Dual Interior Point Filter Line Search Algorithm for Large-Scale Nonlinear Programming." *Mathematical Programming* 106:25–57.

Ward, J. K., J. Wall, S. West, and R. de Dear. 2008. "Beyond Comfort Managing the Impact of HVAC Control on the Outside World." *In Proceedings of Conference: Air Conditioning and the Low Carbon Cooling Challenge*.

Zavala, V. M., D. Skow, T. Celinski, and P. Dickinson. 2011. "Techno-Economic Evaluation of a Next-Generation Building Energy Management System." *Technical Report ANL/MCS-TM-313, Argonne National Laboratory*.

Zavala, V. M., J. Wang, S. Leyffer, E. M. Constantinescu, M. Anitescu, and G. Conzelmann. 2010. "Proactive Energy Management for NExt-Generation Building Systems." *In Proceedings of 4th International Conference of IBPSA-USA*.

NOMENCLATURE

Variables

$m^z(\cdot)$	total air mass in the building, gr_{air}
$C_i^z(\cdot)$	concentration in building air, gr_i/m^3
$C_i^{in,z}(\cdot)$	concentration in inlet air, gr_i/m^3
$C_i^m(\cdot)$	concentration in mixer, gr_i/m^3
$m_i^{rm}(\cdot)$	mass removal rate in AHU, gr_i/hr
$P^z(\cdot)$	building pressure, atm
$ppmV_{CO_2}^z(\cdot)$	CO_2 concentration, $ppmV$
$q^{in,z}(\cdot)$	volumetric inlet flow rate, m^3/hr
$q^{out,z}(\cdot)$	volumetric outlet flow rate, m^3/hr
$q^m(\cdot)$	volumetric flow rate in mixed, m^3/hr
$q^{amb}(\cdot)$	volumetric ambient air flow rate, m^3/hr
$q^{ex}(\cdot)$	volumetric exhaust air flow rate, m^3/hr
$Q^{lat}(\cdot)$	latent heat removed in AHU, kJ/hr
$Q^{sens}(\cdot)$	sensible heat removed in AHU, kJ/hr
$Q^{hvac}(\cdot)$	electrical energy consumed by HVAC, kJ/hr
$T^z(\cdot)$	average temperature in building, K
$T^{in,z}(\cdot)$	temperature of inlet air, K
$T^m(\cdot)$	temperature in mixer, K
$RH^z(\cdot)$	relative humidity in building, %

Data

$C_i^{amb}(\cdot)$	concentration in ambient air, gr_i/m^3
$T^{amb}(\cdot)$	temperature of ambient air, K
n_{tot}	number of occupants, 500
G_i^z	generation rate per occupant $(CO_2 = 2.4, H_2O = 50)\ gr_i/hr$ (Aglan 2003)
Q^z	building heat gain per occupant, 432 kJ/hr
U^w	wall heat-transfer coefficient, 18 $kJ/hr \cdot m^2 \cdot K$
V^z	total building volume, 1000 m^3
A^w	total wall heat-transfer area, 600 m^2
c_p	air heat capacity , $1.0 \times 10^{-3}\ kJ/gr_{air} \cdot K$
h^{lat}	latent heat of condensation, 2.46 kJ/gr_{H_2O}
ρ	air density , 1200 g/m^3
M	air molecular weight, 29 gr/gr_{mol}
M_{CO_2}	CO_2 molecular weight, 44 gr/gr_{mol}
R	universal gas constant, $0.082 \times 10^{-3} atm \cdot m^3/gr_{mol}K$